Composite Structures 204 (2018) 620–633

Contents lists available at ScienceDirect

Composite Structures

journal homepage: www.elsevier.com/locate/compstruct

# A refined quasi-3D zigzag beam theory for free vibration and stability analysis of multilayered composite beams subjected to thermomechanical loading

Bin Han[a,b,c,g], Wei-Wei Hui[d], Qian-Cheng Zhang[b,e], Zhen-Yu Zhao[b,e], Feng Jin[b,e], Qi Zhang[a,*], Tian Jian Lu[f,b,*], Bing-Heng Lu[a]

[a] School of Mechanical Engineering, Xi'an Jiaotong University, Xi'an 710049, China
[b] MOE Key Laboratory for Multifunctional Materials and Structures, Xi'an Jiaotong University, Xi'an 710049, China
[c] School of Engineering, Brown University, Providence, RI 02912, USA
[d] The Fourth Academy of China Aerospace Science and Technology Corporation, Xi'an 710025, China
[e] State Key Laboratory for Strength and Vibration of Mechanical Structures, Xi'an Jiaotong University, Xi'an 710049, China
[f] State Key Laboratory of Mechanics and Control of Mechanical Structures, Nanjing University of Aeronautics and Astronautics, Nanjing 210016, China
[g] Research institute of Xi'an Jiaotong University, Zhejiang, Hangzhou 311215, China

ARTICLE INFO

*Keywords:*
Quasi-3D zigzag beam theory
Layered structure
Vibration
Buckling
Thermomechanical loading

ABSTRACT

A refined four-unknown quasi-3D zigzag beam theory is developed to model the free vibration and buckling behaviors of multilayered composite beams subjected to axial mechanical loading (e.g., distributed load and terminal force) and uniform temperature variation. Types of the composite beams considered include laminated composite beams, sandwich beams with composite face sheets, and fiber metal laminates. The proposed theory accounts for not only thickness stretching but also interlaminar continuity of transverse shear stresses and displacements. Associated eigenvalue problems for various boundary conditions are derived using the Ritz method. Accuracy and effectiveness of the theoretical predictions are verified by comparison with existing results and present finite element simulations. The theory is employed to quantify the effects of axial distributed load/terminal force and temperature variation on free vibration and buckling for different boundary conditions, geometric parameters and material properties. The present theory could produce sufficiently accurate predictions of natural frequencies and buckling capacities of multilayered beams at a very low computational cost.

## 1. Introduction

Lightweight laminated composite and sandwich structures have enjoyed widespread engineering applications due to their superior stiffness, strength, shock resistance and other excellent properties. Fiber metal laminates (FMLs), as a kind of hybrid material made of stacked metal sheets and fiber reinforced composite (FRC) layers [1], have also been increasingly applied as structural material for the aerospace industry (*e.g.*, lower wing skin and internal parts of airplanes, Airbus A380 fuselage, etc.), attributed to their excellent fatigue, impact resistance, and damage tolerance [2]. This research aims to develop a refined four-unknown quasi-3D zigzag beam theory to characterize the free vibration and buckling behaviors of multilayered composite beams (including laminated composite, sandwich and FML beams). The beam is subjected to axial mechanical load, e.g., distributed load and terminal force, and uniform temperature variation.

Existing research on the dynamic response of FMLs has mainly focused on the classical or first-order beam/plate theories. For typical instance, based on the first-order shear deformation theory, Shooshtari and Razavi [3] employed the Galerkin method and multiple time scales method to study linear and nonlinear free vibration behaviors of a FML rectangular panel. Using the first-order shear deformation theory as well as the Fourier series method, Payeganeh et al. [4] investigated the dynamic response of FMLs subjected to low-velocity impact. By adopting the differential quadrature method, Nermark-beta method and iterative method, Fu et al. [5,6] studied the nonlinear dynamic response of delaminated FML beams and viscoelastic FML beams under thermal shock based upon the Timoshenko beam theory. Using the Galerkin method and Newmark method, Tao et al. [7] employed the Euler-Bernoulli beam theory to study nonlinear dynamic behavior of FML beams

* Corresponding authors at: School of Mechanical Engineering, Xi'an Jiaotong University, Xi'an 710049, China (Q. Zhang). State Key Laboratory of Mechanics and Control of Mechanical Structures, Nanjing University of Aeronautics and Astronautics, Nanjing 210016, China (T.J. Lu).
*E-mail addresses:* henryzhang@mail.xjtu.edu.cn (Q. Zhang), tjlu@mail.xjtu.edu.cn (T.J. Lu).

https://doi.org/10.1016/j.compstruct.2018.08.005
Received 7 December 2017; Received in revised form 22 July 2018; Accepted 2 August 2018
Available online 04 August 2018
0263-8223/ 

subjected to moving loads in thermal environment.

Beams subjected to axially distributed load, *e.g.*, self-weight or acceleration-induced body force, are a class of commonly applied structures in civil and aerospace engineering. The axially distributed load plays an important role in affecting the stability and natural frequencies of the structures. As reviewed in our previous work [8], existing research studied the stability or post-buckling of beams subjected to axially distributed load using the classical Euler-Bernoulli beam theory, with the effect of transverse shear ignored. To address this deficiency, Han et al. [8] adopted the Timoshenko theory with both Engesser and Haringx types to study the stability and initial post-buckling of beams subjected to combined axially distributed load and terminal force. It was found that the effect of transverse shear deformation should not be neglected especially for predicting the buckling of sandwich and composite laminated beams, and the Engesser shear theory gave better predictions than the Haringx type.

Existing research on vibration analysis of beams subjected to axially distributed load was mostly carried out within the framework of Euler-Bernoulli and Timoshenko beam theories [9]. For example, taking account of self-weight, Naguleswaran [10] used the Frobenius method to investigate the natural frequencies of standing and hanging Euler-Bernoulli beams. Virgin et al. [11] evaluated the effect of gravity on the vibration of vertical Euler-Bernoulli cantilevers. Employing a multiple time-scales perturbation method, Hijmissen and Horssen [12] studied the vibration of a standing Euler-Bernoulli beam with a tip-mass damper, and later the transverse vibration of a standing, uniform, cantilevered Timoshenko beam [13]. Abramovich [14] utilized the Galerkin method to investigate the free vibration of a hanging Timoshenko beam, while Xi et al. [15] studied the free vibration of a hanging or standing Rayleigh beam-column subjected to vertically oriented gravity load.

At present, higher-order shear deformation theories are scarcely employed to study the vibration and stability of FML beams, or standing laminated and sandwich beams subjected to axially distributed load. The Euler-Bernoulli beam theory, as the simplest deformation beam theory, is inaccurate for reasonably thick and/or highly anisotropic composite beams, as it neglects transverse shear strain in the laminates. Timoshenko beam theory, or the first-order beam theory, considers constant transverse shear strain through the beam thickness and hence has to incorporate a shear correction factor to adjust the transverse shear stiffness. However, while the shear correction factor determines the accuracy, it could not in general be determined a priori apart from very special cases [16,17]. To address this issue, several higher-order shear deformation theories (HSDTs), e.g., polynomial, trigonometric, exponential and hyperbolic shear deformation theories, have been developed as the Equivalent Single Layer (ESL) theories, LayerWise (LW) theories, and Zigzag (ZZ) theories, which have been recently reviewed for laminated composites and sandwich beams [18–22] as well as functionally graded (FG) beams [23–25]. In the frame of one dimensional (1D) LW models, Léotoing et al. [26] investigated the geometrically nonlinear interaction between overall and local buckling modes of sandwich beams, Yu et at. [27] developed a 1D finite element model to simulate the instability of sandwich beams with high efficiency, and Sad Saoud and Le Grognec [28] studied the post-buckling behavior of sandwich beams. In order to minimize the computational cost of the LW models, one can resort to ZZ theories [29]. Kapuria et al. [30] assessed the zigzag theory for static loading, buckling, free and forced response of composite and sandwich beams. Hu et al. [31] evaluated different kinematic theories on the static and dynamic analysis of various sandwich beams with viscoelastic core, and found the zigzag theories were more accurate than classic laminated theory (CLT) and HSDT based ESL models. Carrera et al. [32,33] presented the static and dynamic analysis of laminated beams by using polynomial, trigonometric, exponential, and zigzag functions in the frameworks of the Carrea Unified Formulation. Tessler [34] developed the refined zigzag theory (RZT) based upon the Timoshenko beam theory for laminated composite beams. Referring to the kinematics of Tessler's RZT, Di Sciuva et al. [35] and Treviso et al. [36] developed a class of $C^0$-continuous beam elements for the analysis of laminated beams. The $C^0$-continuous kinematics of the in-plane components satisfying the continuity of transverse stresses can be efficiently reproduced by adopting the zigzag theories. However, most of the Zigzag theories are complicated when thickness expansion is taken into account and the pre-stress is considered under thermal environment.

For thick laminated, sandwich or FG beams, the normal strain effect, regarded as thickness stretching, becomes very important and should be considered in vibration and stability analysis [37]. Using a higher-order shear and normal deformation theory with axial and transverse displacements expanded in power series, Matsunaga [38] studied the vibration and buckling of a simply supported multilayered composite beam subjected to axial stresses. Mantari and Canales [39,40] utilized the Ritz method with hybrid series to study the buckling and vibration of laminated beams with various boundary conditions. To this end, they employed two quasi-3D higher-order shear deformation theories, which include both shear deformation and thickness effects with a higher-order variation of in-plane and out-plane displacements through the thickness. Based upon a refined quasi-3D polynomial theory, Vo et al. [24,41,42] developed analytical solutions and finite element (FE) models to investigate FG and composite laminated beams. Nguyen et al. [43] and Osofero et al. [44] employed a variety of quasi-3D theories to investigate the vibration and buckling of FG sandwich beams. Existing quasi-3D theories are quite applicable to FG beams/plates, as they automatically satisfy the interlaminar continuity of both displacements and transverse shear stresses due to the continuous gradient change of materials along the thickness. However, for multilayered laminated beams, such theories violate the continuity conditions of transverse stresses due to the jump change of material properties at the layered interfaces, usually leading to overestimated prediction of natural frequency and buckling load [45,46]. As emphasized in a recent review [21], in view of minimizing the number of unknown variables, higher-order beam theories considering the effects of both the transverse normal deformation and interlaminar continuous transverse shear stresses on bending, buckling and vibration responses should be developed for laminated composite and sandwich beams.

In the present study, a refined and generalized quasi-3D zigzag beam theory is developed to characterize the free vibration and stability behaviors of composite, sandwich and FML beams with different boundary conditions under axial mechanical (e.g., axially distributed load and terminal force) and thermal loading. In Section 2, the deformation theory is introduced by incorporating a refined four-unknown higher-order shear theory and zigzag-type continuous transverse functions, and accounts for both thickness stretching and interlaminar continuity of transverse shear stresses and displacements, which could produce sufficiently accurate results at low computational cost. The Ritz method in terms of boundary characteristic orthogonal polynomial functions is applied to solve the vibration and buckling problems. For validation, the theoretical predictions are compared with existing literature results and the present FE simulations in Section 3. In Section 4, three situations are considered and analyzed for various multi-layered configurations: (i) sandwich and laminated composite beams with different boundary conditions; (ii) micromechanics-based laminated beams with hinged-hinged boundary condition; (iii) fiber metal laminated (FML) beams with hinged-hinged boundary condition. Lastly, Section 5 closes the paper with conclusions.

## 2. Theoretical formulation

With reference to Fig. 1, consider a symmetric multi-layered composite beam composed of $2N + 1$ layers perfectly bonded together. The beam has length $L$, width $b$, and total thickness $h$. The global coordinate system $x$-$y$-$z$ is chosen such that the $x$-$y$ plane coincides with the mid-plane of the beam. Let the superscript 0 denote all quantities referring

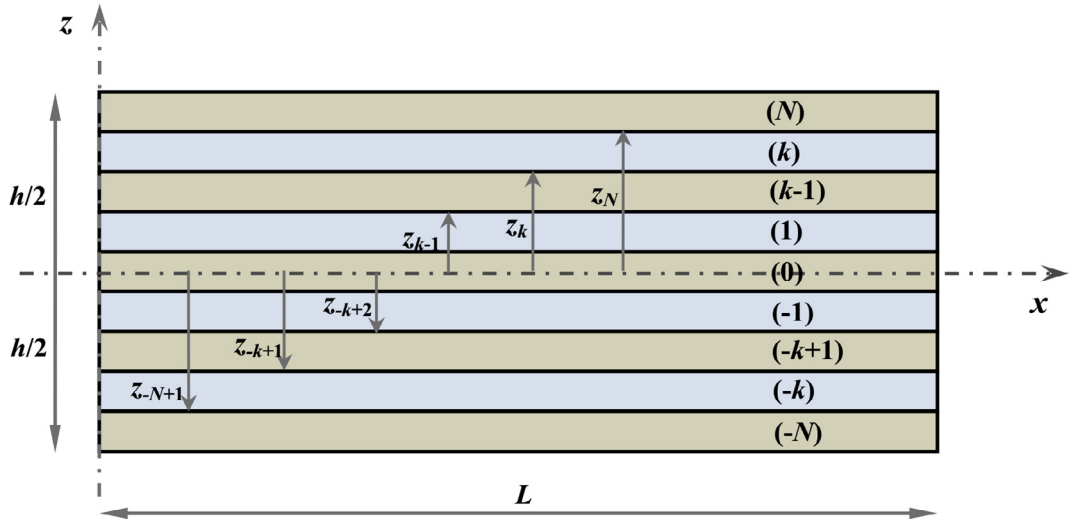


**Fig. 1.** Geometry of a symmetrical multi-layered composite beam and its co-ordinate system.

to the middle-layer or core-layer, and let "$z_k$" denote the material interface coordinate between the $k$-th and ($k$-1)-th layers. The beam may be a laminated composite, a composite sandwich, or a FML structure.

The linear thermoelastic constitutive relations of the $k$-th orthotropic layer/lamina with any fiber orientation with respect to the $x$–$z$ plane may be expressed as:

$$\begin{Bmatrix}\sigma_x\\ \sigma_z\\ \tau_{xz}\end{Bmatrix}^{(k)} = \begin{bmatrix}\overline{Q_{11}} & \overline{Q_{13}} & 0\\ \overline{Q_{13}} & \overline{Q_{33}} & 0\\ 0 & 0 & \overline{Q_{55}}\end{bmatrix}^{(k)} \begin{Bmatrix}\varepsilon_x-\alpha_x\Delta T\\ \varepsilon_z-\alpha_z\Delta T\\ \gamma_{xz}-\alpha_{xz}\Delta T\end{Bmatrix}^{(k)} \tag{1}$$

where $\Delta T$ is temperature change from the stress free state, and a uniform temperature variation is assumed. While detailed expressions of the well-known reduced stiffness $\overline{Q_{ij}}$ can be found in [47], the coefficients of thermal expansion for the $k$-th layer in the laminated reference coordinates are:

$$(\alpha_x,\ \alpha_z,\ \alpha_{xz}) = (\cos^2\theta\ \alpha_1 + \sin^2\theta\ \alpha_2,\ \alpha_3,\ 0) \tag{2}$$

where $\theta$ is the angle between the fiber direction and the $x$-axis of the individual layer.

### 2.1. Deformation field with quasi-3D shear deformation beam theory

The displacement field is constructed on the basis of a refined and generalized quasi-3D shear and normal deformable beam theory developed from Mohammed [42,48,49]. The in-plane displacement $u(x, z, t)$ is expanded as odd functions of the thickness coordinate while the transverse displacement $w(x, z, t)$ is splitted into bending, shear and thickness stretching parts, as:

$$\begin{cases}u(x,z,t) = u_0(x,t)-zw_{b,x}-f(z)w_{s,x}\\ w(x,z,t) = w_b(x,t) + w_s(x,t) + g(z)\varphi_z(x,t)\end{cases} \tag{3}$$

where $u_0(x, t)$, $w_b(x, t)$, $w_s(x, t)$ and $\varphi_z(x, t)$ are the four unknown functions of the beam, $f(z)$ is the shape function determining transverse shear strains along the thickness, and $g(z) = 1-f'(z)$. A prime denotes the derivative with respect to $z$, and the subscript "$x$" represents the partial derivative with respect to $x$. As a compact formulation, the above displacement field can take into account different higher-order shear deformation functions, satisfying the stress free boundaries at the top and bottom surfaces. However, within the frame of this quasi-3D shear deformation beam theory, the transverse stresses are not continuous at the interface between two neighboring layers.

### 2.2. Kinematics with improved quasi-3D zigzag shear deformation beam theory

With the $k$-th layer taken as an independent beam ($k = 0,\ \pm1,\ ...,\pm N$), its displacement components can be written as:

$$\begin{cases}u^{(k)}(x,z,t) = u_0^{(k)}-zw_{b,x}^{(k)}-f^{(k)}(z)w_{s,x}^{(k)}\\ w^{(k)}(x,z,t) = w_b^{(k)} + w_s^{(k)} + g^{(k)}(z)\varphi_z^{(k)}\end{cases} \tag{4}$$

where $g^{(k)}(z) = 1-f^{(k)\prime}(z)$. In the present study, small elastic deformations are assumed, i.e., displacements and rotations are small, and they obey Hooke's law. The strain field can be expressed as:

$$\begin{cases}\varepsilon_x^{(k)} = u_{0,x}^{(k)}-zw_{b,x}^{(k)}-f^{(k)}(z)w_{s,xx}^{(k)}\\ \varepsilon_x^{(k)} = g^{(k)\prime}(z)\varphi_z^{(k)},\ \gamma_{xz}^{(k)} = g^{(k)}(z)(w_{s,x}^{(k)} + \varphi_{(x,x)}^{(k)})\end{cases} \tag{5}$$

From Eqs. (1) and (5), the transverse shear stress of the $k$-th layer can be obtained as:

$$\tau_{xz}^{(k)} = Q_{55}^{(k)}g^{(k)}(z)(w_{s,x}^{(k)} + \varphi_{z,x}^{(k)}) \tag{6}$$

It is assumed that

$$\begin{aligned}w_s^{(k)} &= A_k w_s^{(0)} + B_k\varphi_z^{(0)}\\ \varphi_z^{(k)} &= C_k\varphi_z^{(0)}\end{aligned} \tag{7}$$

Upon inserting (7) into (6), the requirement of continuity of interlaminar shear stress at $z_k$ yields:

$$\begin{aligned}A_k &= \frac{Q_{55}^{(k\mp1)}g^{(k\mp1)}(z_k)}{Q_{55}^{(k)}g^{(k)}(z_k)}A_{k\mp1},\quad A_0 = 1\\ B_k &= \frac{Q_{55}^{(k\mp1)}g^{(k\mp1)}(z_k)}{Q_{55}^{(k)}g^{(k)}(z_k)}(B_{k\mp1} + C_{k\mp1})-C_k,\quad B_0 = 0,\ C_0 = 1\end{aligned} \tag{8}$$

where the upper or lower sign on the right side is connected with the negative or positive values of $k$, respectively. Substituting Eq. (7) into Eq. (4) and maintaining continuity of displacement components (i.e., $u^{(k)}$ and $w^{(k)}$) at $z_k$ yields:

$$\begin{aligned}w_b^{(k)} &= w_b^{(0)} + (1-A_k)w_s^{(0)}-B_k\varphi_z^{(0)}\\ u_0^{(k)} &= u_0^{(0)} + D_k w_{s,x}^{(0)} + E_k\varphi_{z,x}^{(0)}\end{aligned} \tag{9}$$

where

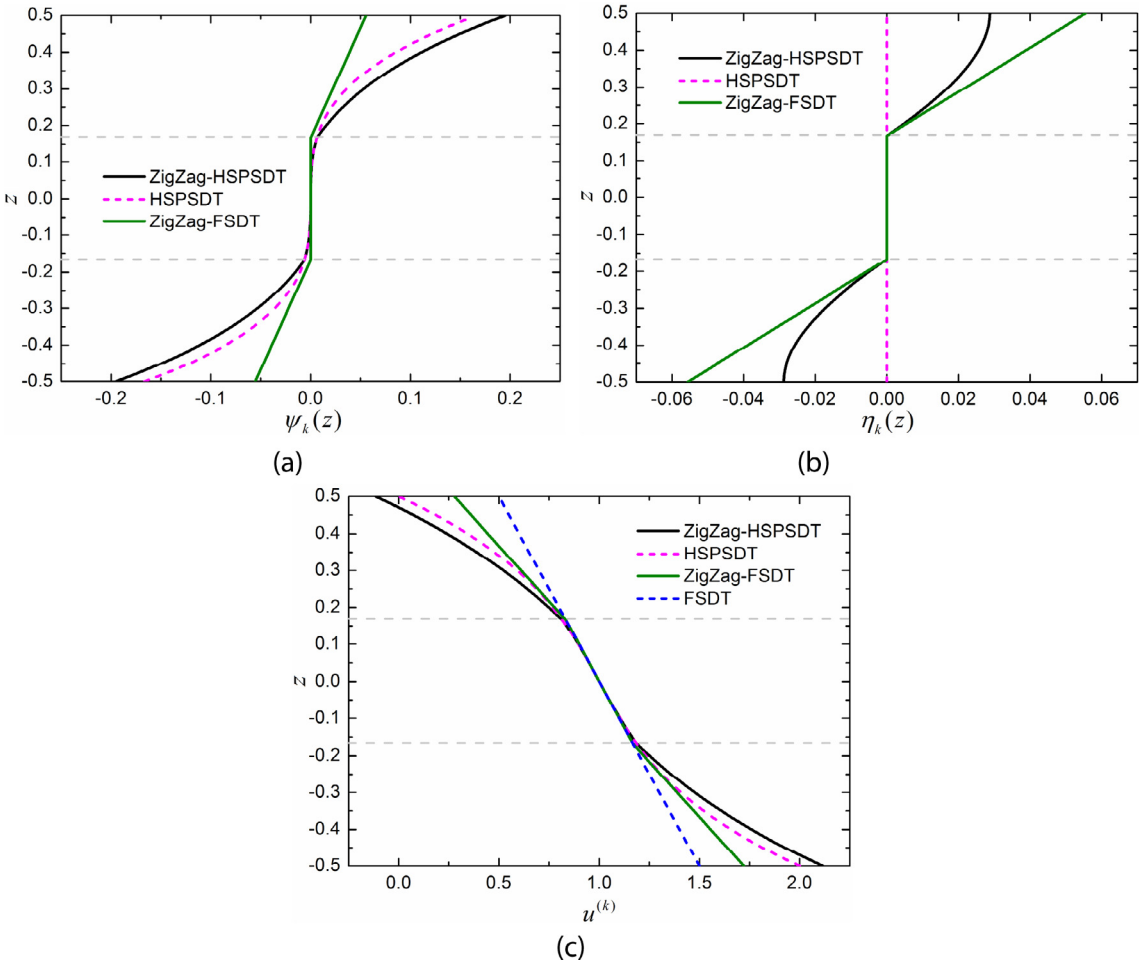


**Fig. 2.** Schematic representation of the proposed refined zigzag higher-order shear beam theory. Thickness distribution of zigzag function (a) $\psi_k(z)$, (b) $\eta_k(z)$, and zigzag axial displacement (c) $u^{(k)}$ of a three-layered laminated beam.

$$
\begin{aligned}
&C_k = \frac{g^{(k\mp1)}(z_k)}{g^{(k)}(z_k)} C_{k\mp1},\\
&D_k = D_{k\mp1} + z_k(A_{k\mp1} - A_k) + f^{(k)}(z_k)A_k - f^{(k\mp1)}(z_k)A_{k\mp1},\quad D_0 = 0\\
&E_k = E_{k\mp1} + z_k(B_{k\mp1} - B_k) + f^{(k)}(z_k)B_k - f^{(k\mp1)}(z_k)B_{k\mp1},\quad E_0 = 0
\end{aligned}
\tag{10}
$$

As a result of the forgoing definitions, the displacement components of all the constituent layers have been written in terms of the corresponding components of the middle layer. Inserting Eqs. (7)–(10) into Eq. (4), an improved quasi-3D zigzag shear deformation beam theory is obtained as:

$$
\begin{cases}
u^{(k)} = u_0^{(0)} - z w_{b,x}^{(0)} + [D_k - z(1 - A_k) - f^{(k)}(z)A_k] w_{s,x}^{(0)} \\
\qquad\quad + [E_k + z B_k - f^{(k)}(z) B_k] \varphi_{z,x}^{(0)} \\
w^{(k)} = w_b^{(0)} + w_s^{(0)} + g^{(k)}(z) C_k \varphi_z^{(0)}
\end{cases}
\tag{11}
$$

This form of displacement approximation yields continuous displacements and transverse shear stress throughout the multi-layered beam thickness, regardless of any a posteriori specified shape function $f^{(k)}(z)$. Let

$$
f^{(k)}(z) = f(z), \quad g^{(k)}(z) = g(z) = 1 - f'(z)
\tag{12}
$$

It follows that Eqs. (8) and (10) can be reduced to

$$
\begin{aligned}
&A_k = \frac{Q_{55}^{(k\mp1)}}{Q_{55}^{(k)}} A_{k\mp1},\quad C_k = 1,\quad B_k = \frac{Q_{55}^{(k\mp1)}}{Q_{55}^{(k)}}(B_{k\mp1} + 1) - 1\\
&D_k = D_{k\mp1} + [z_k - f(z_k)](A_{k\mp1} - A_k)\\
&E_k = E_{k\mp1} + [z_k - f(z_k)](B_{k\mp1} - B_k)\\
&A_0 = 1, \qquad B_0 = D_0 = E_0 = 0
\end{aligned}
\tag{13}
$$

where $A_k$ and $B_k$ are dependent on layer sequence and material properties, while $D_k$ and $E_k$ are additionally determined by the thickness coordinate and shear shape function. Therefore, Eq. (11) can be rewritten as:

$$
\begin{cases}
u^{(k)}(x, z; t) = u_0 - z w_{b,x} - \psi_k(z) w_{s,x} - \eta_k(z) \varphi_{z,x} \\
w^{(k)} = w_b + w_s + g(z) \varphi_z
\end{cases}
\tag{14}
$$

where $u_0^{(0)}$, $w_b^{(0)}$, $w_s^{(0)}$, and $\phi_z^{(0)}$ are replaced by $u_0$, $w_b$, $w_s$, and $\phi_z$, respectively; $\psi_k(z)$ and $\eta_k(z)$ denote two piecewise zigzag functions, expressed as

$$
\begin{aligned}
\psi_k(z) &= f(z)A_k + z(1 - A_k) - D_k\\
\eta_k(z) &= f(z)B_k - z B_k - E_k
\end{aligned}
\tag{15}
$$

Upon setting $f(z) = 0$, the zigzag first-order (linear) shear deformation beam theory (FSDT) is obtained. On the other hand, by taking $\psi_k(z) = f(z)$ and $\eta_k(z) = 0$, Eq. (14) is reduced to the quasi-3D shear deformation beam theory of Eq. (3), as a kind of equivalent single layer (ESL) theories. In the present study, a combined hyperbolic sinusoidal and polynomial shape function for the quasi-3D zigzag shear deformation beam theory (HSPSDT) [49], as illustrated in Fig. 2, is chosen as: Fig. 3

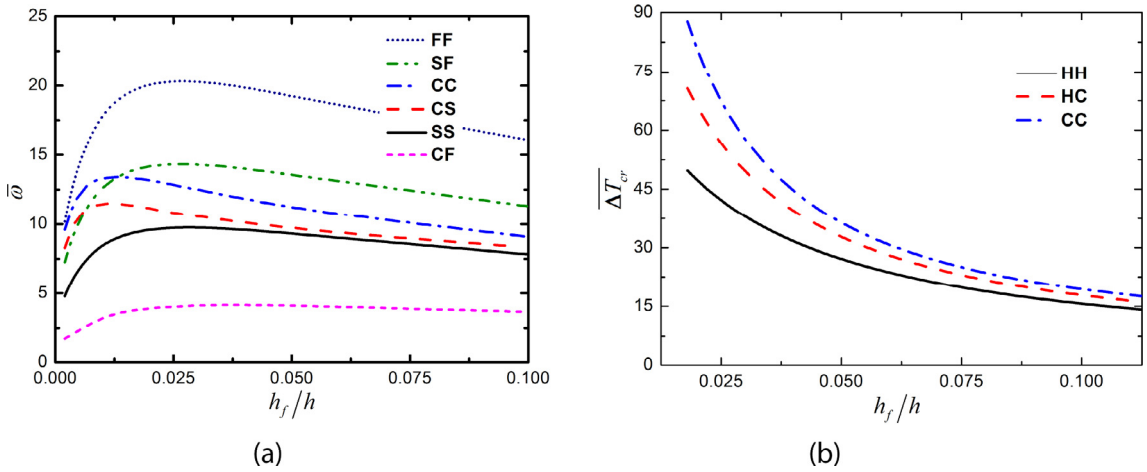


(a) (b)

**Fig. 3.** Effect of face-to-thickness ratio $h_f/h$ on (a) fundamental frequency and (b) critical temperature variation of sandwich beams ([*face*/*core*/*face*], $L/h = 5$, Material 3) with selected boundary conditions.

$$f(z) = z - h\sinh\left(\frac{z}{h}\right) + \frac{4}{3}\frac{z^3}{h^2}\cosh\left(\frac{1}{2}\right) \tag{16}$$

Based on this formulation, the strain-displacement relationships are: Fig. 4

$$\begin{aligned} \varepsilon_x &= \varepsilon_{x0} + zk_x^b + \psi_k(z)k_x^s + \eta_k(z)k_x^{st} \\ \varepsilon_z &= g'(z)\varepsilon_{z0}, \quad \gamma_{xz} = g(z)\gamma_{xz0} \end{aligned} \tag{17}$$

where

$$\begin{aligned} &\varepsilon_{x0} = u_{0,x},\ k_x^b = -w_{b,xx},\ k_x^s = -w_{s,xx},\ k_x^{st} = -\varphi_{z,xx},\ \varepsilon_{z0} = \varphi_z,\ \gamma_{xz0} \\ &= w_{s,x} + \varphi_{z,x} \end{aligned} \tag{18}$$

In contrast to the displacement field of Eq. (3), the quasi-3D zigzag shear deformation beam theory of Eq. (14) allows the interlaminar continuity of transverse shear stresses. It should also be noted that all interface and boundary conditions are exactly satisfied for displacements and transverse shear stress.

### 2.3. Stress resultants

The constitutive equations relating the force and moment resultants to strains and curvatures of the reference surface are given in the following form:

$$\begin{aligned} \begin{Bmatrix} N_x \\ M_x^b \\ M_x^s \\ M_x^{st} \end{Bmatrix} &= \int_{-h/2}^{h/2} \sigma_x^{(k)} \begin{Bmatrix} 1 \\ z \\ \psi_k(z) \\ \eta_k(z) \end{Bmatrix} \mathrm{d}z, \quad S_{xz} = \int_{-h/2}^{h/2} \tau_{xz}^{(k)} g(z)\mathrm{d}z, \quad N_z \\ &= \int_{-h/2}^{h/2} \sigma_z^{(k)} g'(z)\mathrm{d}z \end{aligned} \tag{19}$$

Upon inserting (14) and (17) into (19), the force and moment resultants are written as:

$$\begin{aligned} &\begin{Bmatrix} N_x \\ M_x^b \\ M_x^s \\ M_x^{st} \end{Bmatrix} = \begin{bmatrix} A_{11} & A_{11}^b & A_{11}^s & A_{11}^{st} \\ A_{11}^b & B_{11}^b & B_{11}^s & B_{11}^{st} \\ A_{11}^s & B_{11}^s & C_{11}^s & C_{11}^{st} \\ A_{11}^{st} & B_{11}^{st} & C_{11}^{st} & D_{11}^{st} \end{bmatrix} \begin{Bmatrix} \varepsilon_{x0} \\ k_x^b \\ k_x^s \\ k_x^{st} \end{Bmatrix} + \begin{bmatrix} L_1 \\ L_1^b \\ L_1^s \\ L_1^{st} \end{bmatrix} \varepsilon_{z0} - \begin{Bmatrix} N_x^T \\ M_x^{bT} \\ M_x^{sT} \\ M_x^{stT} \end{Bmatrix}, \\ &S_{xz} = A_{55}^s \gamma_{xz0} \\ &N_z = L_1\varepsilon_{x0} + L_1^b k_x^b + L_1^s k_x^s + L_1^{st} k_x^{st} + R^s\varepsilon_{z0} - N_z^T \end{aligned} \tag{20}$$

where

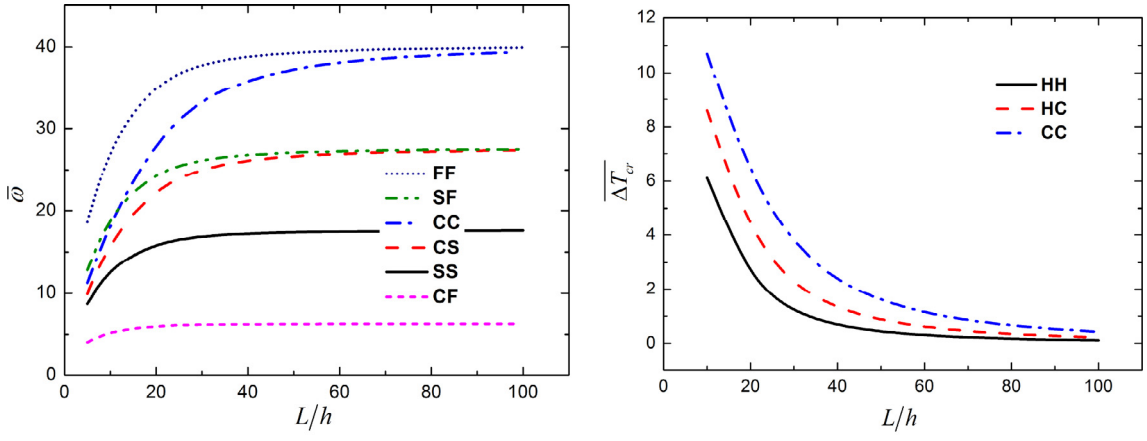


(a) (b)

**Fig. 4.** Effect of length-to-thickness ratio $L/h$ on (a) fundamental frequency and (b) critical temperature variation of laminated beams ([0°/90°/0°], Material 1) with selected boundary conditions.

$$\begin{bmatrix} A_{11} & A_{11}^b & A_{11}^s & A_{11}^{st} \\ A_{11}^b & B_{11}^b & B_{11}^s & B_{11}^{st} \\ A_{11}^s & B_{11}^s & C_{11}^s & C_{11}^{st} \\ A_{11}^{st} & B_{11}^{st} & C_{11}^{st} & D_{11}^{st} \end{bmatrix} = \int_{-h/2}^{h/2} \begin{bmatrix} 1 & z & \psi_k(z) & \eta_k(z) \\ & z^2 & z\psi_k(z) & z\eta_k(z) \\ \text{Symmetry} & & \psi_k^2(z) & \psi_k(z)\eta_k(z) \\ & & & \eta_k^2(z) \end{bmatrix} \bar{Q}_{11}^{(k)} \mathrm{d}z$$

$$\begin{Bmatrix} L_1 \\ L_1^b \\ L_1^s \\ L_1^{st} \end{Bmatrix} = \int_{-h/2}^{h/2} \begin{bmatrix} 1 \\ z \\ \psi_k(z) \\ \eta_k(z) \end{bmatrix} g'(z) \bar{Q}_{13}^{(k)} dz, \quad \begin{Bmatrix} N_x^T \\ M_x^{bT} \\ M_x^{sT} \\ M_x^{stT} \end{Bmatrix} = \int_{-h/2}^{h/2} \begin{Bmatrix} 1 \\ z \\ \psi_k(z) \\ \eta_k(z) \end{Bmatrix} (\alpha_x \overline{Q_{11}} + \alpha_z \overline{Q_{13}})^{(k)} \Delta T dz$$

$$N_z^T = \int_{-h/2}^{h/2} g'(z)(\alpha_x \overline{Q_{13}} + \alpha_z \overline{Q_{33}})^{(k)} \Delta T dz$$

$$R^s = \int_{-h/2}^{h/2} \bar{Q}_{33}^{(k)} (g'(z))^2 dz, \quad A_{55}^s = \int_{-h/2}^{h/2} g^2(z) \bar{Q}_{55}^{(k)} \ \mathrm{d}z \tag{21}$$

### 2.4. Ritz solution of vibration and stability problems

The Ritz method provides a convenient methodology for obtaining approximate solutions to boundary value problems. This approach is equally applicable to the buckling and free vibration problems of multi-layered composite beams. In the present study, application of the Ritz method requires the total potential energy $\prod$:

$$\prod = U + V - T \tag{22}$$

where $U$ is the strain energy, $T$ denotes the kinetic energy, and $V$ refers to the potential energies of external axial forces induced by thermal or mechanical loading. The strain energy of a multi-layered composite beam can be expressed as:

$$U = \frac{1}{2}\int_V [\sigma_x \varepsilon_x + \sigma_z \varepsilon_z + \tau_{xz}\gamma_{xz}]\mathrm{d}V = \frac{1}{2} b \int_0^L \begin{bmatrix} A_{11}(\varepsilon_{x0})^2 + 2A_{11}^b \varepsilon_{x0} k_x^b + 2A_{11}^s \varepsilon_{x0} k_x^s + 2A_{11}^{st} \varepsilon_{x0} k_x^{st} \\ \quad + 2L_1 \varepsilon_{x0} \varepsilon_{z0} + B_{11}^b (k_x^b)^2 + 2B_{11}^s k_x^b k_x^s + 2B_{11}^{st} k_x^b k_x^{st} \\ + 2L_1^b k_x^b \varepsilon_{z0} + C_{11}^s (k_x^s)^2 + 2C_{11}^{st} k_x^s k_x^{st} + 2L_1^s k_x^s \varepsilon_{z0} \\ \quad + D_{11}^{st} (k_x^{st})^2 + 2L_1^{st} k_x^{st} \varepsilon_{z0} + R^s (\varepsilon_{z0})^2 + A_{55}^s (\gamma_{xz0})^2 \end{bmatrix} \mathrm{d}x \tag{23}$$

The potential energy of external axial load $\hat{N}_x$ due to uniform temperature variation or axially mechanical loading can be written as:

$$V_1 = -\frac{1}{2} b \int_0^L \hat{N}_x \left(\frac{\partial w^{(0)}}{\partial x}\right)^2 \mathrm{d}x = -\frac{1}{2} b \int_0^L \hat{N}_x (w_{b,x} + w_{s,x} + g(0)\varphi_{z,x})^2 \mathrm{d}x \tag{24}$$

where $\hat{N}_x = N_x^T$ for thermal loading or $\hat{N}_x = P + q(L-x)$ for axial mechanical loading, which acts along the central axis of the beam. Here, $q$ and $P$ refer to the axially distributed load and terminal force, respectively.

The kinematic energy $T$ of the beam is:

$$T = \frac{1}{2}\int_V \rho(\dot{u}^2 + \dot{w}^2)\mathrm{d}V = \frac{1}{2} b \int_0^L \begin{bmatrix} I_{11}\dot{u}_0^2 + 2I_{12}\dot{u}_0\dot{w}_{b,x} + 2I_{13}\dot{u}_0\dot{w}_{s,x} + 2I_{14}\dot{u}_0\dot{\varphi}_{z,x} + I_{22}\dot{w}_{b,x}^2 \\ \quad + 2I_{23}\dot{w}_{b,x}\dot{w}_{s,x} + 2I_{24}\dot{w}_{b,x}\dot{\varphi}_{z,x} \\ + I_{33}\dot{w}_{s,x}^2 + +2I_{34}\dot{w}_{s,x}\dot{\varphi}_{z,x} + I_{44}\dot{\varphi}_{z,x}^2 \\ \quad + I_{55}(\dot{w}_b^2 + \dot{w}_s^2 + 2\dot{w}_b\dot{w}_s) + 2I_{56}(\dot{w}_b + \dot{w}_s)\dot{\varphi}_z + I_{66}\dot{\varphi}_z^2 \end{bmatrix} \mathrm{d}x \tag{25}$$

where

$$\begin{bmatrix} I_{11} & I_{12} & I_{13} & I_{14} & 0 & 0 \\ I_{12} & I_{22} & I_{23} & I_{24} & 0 & 0 \\ I_{13} & I_{23} & I_{33} & I_{34} & 0 & 0 \\ I_{14} & I_{24} & I_{34} & I_{44} & 0 & 0 \\ 0 & 0 & 0 & 0 & I_{55} & I_{56} \\ 0 & 0 & 0 & 0 & I_{56} & I_{66} \end{bmatrix} = \int_{-h/2}^{h/2} \begin{bmatrix} 1 & -z & -\psi_k(z) & -\eta_k(z) & 0 & 0 \\ & z^2 & z\psi_k(z) & z\eta_k(z) & 0 & 0 \\ & & \psi_k^2(z) & \psi_k(z)\eta_k(z) & 0 & 0 \\ & & & \eta_k^2(z) & 0 & 0 \\ \text{Symmetry} & & & & 1 & g(z) \\ & & & & & g^2(z) \end{bmatrix} \rho(z)\mathrm{d}z \tag{26}$$

In the present study, the adopted admissible Ritz functions which satisfy at least the geometric boundary conditions for deflections and rotations of the beam are given by:

$$\begin{aligned} u_0(\xi, t) &= \sum_{n=1}^{I} c_n \phi_n^c(\xi) \sin\omega t \\ w_b(\xi, t) &= \sum_{m=1}^{R} d_n \phi_n^d(\xi) \sin\omega t \\ w_s(\xi, t) &= \sum_{m=1}^{L} e_n \phi_n^e(\xi) \sin\omega t \\ \varphi_z(\xi, t) &= \sum_{m=1}^{J} f_n \phi_n^f(\xi) \sin\omega t \end{aligned} \tag{27}$$

where $c_n$, $d_n$, $e_n$, $f_n$ are unknown undetermined coefficients, $\xi = x/L$is the non-dimensional coordinate, and the basic functions are defined as

$$\{\phi_n^c(\xi),\ \phi_n^d(\xi),\ \phi_n^e(\xi),\ \phi_n^f(\xi)\} = \{\xi^{i_0},\ \xi^{r_0},\ \xi^{l_0},\ \xi^{j_0}\}\xi^{n-1}(\xi-1)^B \tag{28}$$

The value of $B$ is taken as 0, 1, or 2, which corresponds to free (F), simply supported (S)/hinged (H), and clamped (C) edge conditions, respectively [50]. The displacement components in the Ritz method should satisfy the edge boundary conditions, as tabulated in Table 1. Nine different boundary conditions are considered, namely: FF, SF, SS, SC, CF, CS, CC, HH and HC. It is noticed that if loaded by the axially distributed load, the loading direction points from the second end to the first end, e.g., from S-end to C-end for CS cases. (Here, SC and CS are different for beams under axially distributed load). The kinematic boundary conditions given in Table 1 can be satisfied by careful selection of specific indices (*i.e.*, $i_0$, $r_0$, $l_0$, $j_0$) of the series in Eq. (28), with details illustrated in Table 2 for the boundary conditions considered. Free boundary conditions are approximately satisfied. In the present study, the upper limits of the series in Eq. (27) are defined to be equal, *i.e.*, $I = R = L = J$, which determine the convergence of the following vibration or buckling problems.

According to the Ritz method, minimizing the total potential energy with respect to unknown displacement parameters yields

$$\left\langle \frac{\partial \prod}{\partial c_n}, \frac{\partial \prod}{\partial d_n}, \frac{\partial \prod}{\partial f_n}, \frac{\partial \prod}{\partial e_n} \right\rangle = \langle 0,\ 0,\ 0,\ 0 \rangle \tag{29}$$

Substitution of Eq. (27) into Eqs. (22)–(26) and then into Eq. (29), yields the $4I$ dynamic equations as the following eigenvalue problem:

$$([\mathrm{K}] - [\mathrm{K_G}] - \omega^2[\mathrm{M}])\{\Delta\} = 0 \tag{30}$$

**Table 1**
Kinematic conditions corresponding to different beam end conditions.

| Boundary condition type | At $\xi$ = 0, 1 |
|---|---|
| Simply supported (S) | $u_0 \neq 0$, $w_b = w_s = \varphi_z = 0$ |
| Clamped (C) | $u_0 = w_b = w_s = \varphi_z = w_{b,\xi} = w_{s,\xi} = \varphi_{z,\xi} = 0$ |
| Free (F) | $u_0 \neq 0$, $w_b \neq 0$, $w_s \neq 0$, $\varphi_z \neq 0$ (no constraints) |
| Hinged (H) | $u_0 = 0$, $w_b = w_s = \varphi_z = 0$ |

**Table 2**
Displacement field indices for different boundary conditions.*

| Boundary condition | $i_0$ | $r_0$ | $l_0$ | $j_0$ | $B$ |
|---|---|---|---|---|---|
| FF | 0 | 0 | 0 | 0 | 0 |
| SF | 0 | 1 | 1 | 1 | 0 |
| SS | 0 | 1 | 1 | 1 | 1 |
| SC | 0 | 1 | 1 | 1 | 2 |
| CF | 1 | 2 | 2 | 2 | 0 |
| CS | 1 | 2 | 2 | 2 | 1 |
| CC | 1 | 2 | 2 | 2 | 2 |
| HH | 1 | 1 | 1 | 1 | 1 |
| HC | 1 | 1 | 1 | 1 | 2 |

* In the present study, HH and HC boundary conditions are only discussed for beams under thermal loading.

where [**K**] is the structural stiffness matrix, [$\mathbf{K_G}$] is the geometric stiffness matrix induced by external axial load (i.e., thermal stress, or axially distributed load and terminal force), [**M**] denotes the mass matrix, and Δ refers to the column vector of unknown coefficients of Eq. (27). For stability analysis, Eq. (30) is reduced to:

$$([K]-[K_G])\{\Delta\} = 0 \tag{31}$$

For the present study, although all the eigenvalues and eigenvectors can be computed using the above method for each deformation mode, special focus is placed upon the dominant eigenvalues corresponding to the lowest natural frequencies $\omega$ and minimum critical temperature variations $\Delta T_{cr}$ or critical buckling load $P_{cr}$ or $q_{cr}$. For vibration and buckling analysis, it has been demonstrated that convergence of the present solutions can be ensured with the selected upper limit of series $I$ not exceeding 10.

## 3. Validation studies

### 3.1. Comparison with literature results

In this section, the theories denoted with superscripts 'ds' and 'cs' correspond to the cases that consider discontinuous interlaminar stresses and continuous interlaminar stresses, respectively. The natural frequencies, critical temperature changes and buckling loads predicted by the present quasi-3D zigzag theory (*i.e.*, HSPSDT) are compared with existing results in Tables 4–9, with relevant material properties listed in Table 3. The numbers in parentheses in these tables refer to the percentage errors of the present results relative to those from the literature. Tables 4–7 present dimensionless natural frequencies of laminated and sandwich beams for selected length-to-thickness ratios $L/h$, fiber-stacking sequences, vibration modal $m$ and boundary conditions. Tables 8 and 9 present dimensionless critical temperature variations and critical buckling terminal forces of laminated beams with different boundary conditions.

It is observed from Tables 4–6 and 8 that the natural frequencies and critical buckling temperature variations obtained with the continuous theory take the lower values than the corresponding discontinuous case, which are consistent with the results of Aydogdu [18,19]. Tables 4 and 8 show that the present theory with thickness expansion included predicts slightly lower natural frequencies and critical temperature variations relative to those obtained with the theory neglecting thickness stretching [18,19]. The results of Tables 5 and 6 demonstrate that, HSPSDT$_{cs}$ could provide accurate predictions of natural frequencies (even for the higher-order vibration modals), compared with those obtained using 3D elasticity solutions [51,52]. As tabulated in Tables 7 and 9, comparison of the present HSPSDT$_{cs}$ with

**Table 3**
Material properties used in the present study.

*Material 1*
$E_1/E_2$=open, $E_3 = E_2$, $G_{12} = G_{13} = 0.6E_2$, $G_{23} = 0.5E_2$, $\upsilon_{12} = \upsilon_{13} = \upsilon_{23} = 0.25$, $\alpha_2/\alpha_1 = 3$, $\alpha_3 = \alpha_2$

*Material 2*
$E_1 = 181\text{GPa}$, $E_2 = E_3 = 10.3\text{GPa}$, $G_{12} = G_{13} = 7.17\text{GPa}$, $G_{23} = 2.87\text{GPa}$, $\upsilon_{12} = \upsilon_{13} = \upsilon_{23} = 0.25$, $\rho = 1578\text{kg/m}^3$

*Material 3*

*Face sheets*
$E_1 = 131.1\text{GPa}$, $E_2 = E_3 = 6.9\text{GPa}$, $G_{12} = 3.588\text{GPa}$, $G_{13} = 3.088\text{GPa}$, $G_{23} = 2.3322\text{GPa}$, $\upsilon_{12} = \upsilon_{13} = 0.32$, $\upsilon_{23} = 0.49$, $\rho = 1000\text{kg/m}^3$, $\alpha_2/\alpha_1 = 3$, $\alpha_3 = \alpha_2$

*Core**
$E_1 = 0.2208\text{MPa}$, $E_2 = 0.2001\text{MPa}$, $E_3 = 2760\text{MPa}$, $G_{12} = 16.56\text{MPa}$, $G_{13} = 545.1\text{MPa}$, $G_{23} = 455.4\text{MPa}$, $\upsilon_{12} = 0.99$, $\upsilon_{13} = \upsilon_{23} = 0.00003$, $\rho = 70\text{kg/m}^3$, $\alpha_1/\alpha_{2f} = 1.36$, $\alpha_2/\alpha_1 = 3$, $\alpha_3 = \alpha_2$

*Material 4*

*Fiber*
$E_{f1} = 796.552\text{GPa}$, $E_{f2} = 7.241\text{GPa}$, $G_{f12} = 6.897\text{GPa}$, $G_{f23} = 2.621\text{GPa}$, $\upsilon_{f12} = 0.2$, $\upsilon_{f23} = 0.4$, $\rho_f = 2100\text{kg/m}^3$, $\alpha_{f1} = -1.404 \times 10^{-6}/°\text{C}$, $\alpha_{f2} = 6.84 \times 10^{-6}/°\text{C}$ *Epoxy*
$E_m = (4.345-0.003\Delta T)\text{GPa}$, $\upsilon_m = 0.37$, $\rho_m = 1304\text{kg/m}^3$, $\alpha_m = 43.92 \times (1 + 0.001\Delta T) \times 10^{-6}/°\text{C}$

*Material 5*

Al layer (*Al2024-T3*)
$E = 72.4\text{GPa}$, $G = 27.6\text{GPa}$, $\upsilon = 0.33$, $\rho = 2780\text{kg/m}^3$, $\alpha = 22.4 \times 10^{-6}/°\text{C}$GFRP layer (*Glass-polyster*)
$E_1 = 24.51\text{GPa}$, $E_2 = E_3 = 7.77\text{GPa}$, $G_{12} = G_{13} = 3.34\text{GPa}$, $G_{23} = 1.34\text{GPa}$, $\upsilon_{12} = \upsilon_{13} = \upsilon_{23} = 0.078$
$\rho = 1800\text{kg/m}^3$, $\alpha_1 = 6.34 \times 10^{-6}/°\text{C}$, $\alpha_2 = 23.3 \times 10^{-6}/°\text{C}$, $\alpha_3 = \alpha_2$

* For Material 3, $\alpha_{2f}$ refers to the thermal expansion coefficient of face sheet along the 2-principal direction of material.

**Table 4**
Comparison of non-dimensional fundamental frequencies $\bar{\omega} = (\omega L^2/h)\sqrt{\rho/E_2}$ of a three-layer symmetric cross-ply laminated beam ([0°/90°/0°], $E_1/E_2 = 40$, Material 1).*

| L/h | Theory | Boundary condition | | | | | |
|---|---|---|---|---|---|---|---|
| | | FF | CC | SF | CS | SS | CF |
| 5 | $A_{ds}$ | 19.391 | 11.637 | 13.538 | 10.236 | 9.207 | 4.233 |
| | $HSPSDT_{ds}$ | 19.296 (−0.490) | 11.511 (−1.083) | 13.526 (−0.089) | 10.530 (2.872) | 9.211 (0.043) | 4.228 (−0.118) |
| | $A_{cs}$ | 18.976 | 11.446 | 13.206 | 10.032 | 8.968 | 4.158 |
| | $HSPSDT_{cs}$ | 18.663 (−1.649) | 11.205 (−2.106) | 12.790 (−3.150) | 9.924 (−1.077) | 8.719 (−2.777) | 4.057 (−2.429) |
| 20 | $A_{ds}$ | 36.285 | 29.926 | 25.180 | 22.907 | 16.337 | 6.070 |
| | $HSPSDT_{ds}$ | 36.288 (0.008) | 29.675 (−0.839) | 25.183 (0.012) | 23.364 (1.995) | 16.340 (0.018) | 6.068 (−0.033) |
| | $A_{cs}$ | 36.024 | 29.407 | 25.005 | 22.637 | 16.237 | 6.052 |
| | $HSPSDT_{cs}$ | 35.776 (−0.688) | 28.647 (−2.584) | 24.843 (−0.649) | 22.853 (0.954) | 16.145 (−0.567) | 6.032 (−0.330) |

* A: Results from [19].

alternative quasi-3D higher-order shear theory [40] shows that the Zigzag theory gives slightly lower predictions of natural frequencies and critical buckling load for beams with all kinds of angle-ply laminations and boundary conditions. However, the errors between the frequencies calculated using the two theories are large for the case of SF boundary condition.

### 3.2. Finite element validation

To further ensure the validity and accuracy of the method presented in this paper, finite element (FE) simulations via the commercially available FE code ABAQUS are carried out. Eight-noded plane strain quadrilateral elements with reduced integration (CPE8R) are used, with mesh convergence guaranteed for each calculation. Perfect bonding between two adjacent layers is assumed. The linear perturbation analysis is applied to extract the natural frequency, critical temperature variation, or critical buckling load, similar to [8,53]. Specifically, to determine the stability of beams under combined axially distributed load and terminal force, or the vibration of beams under axial mechanical or thermal loading, a two-step analysis is employed: a general step of static analysis is firstly carried out for calculating the initial stress field under the prescribed axially distributed load, terminal force or uniform temperature variation; subsequently, a linear perturbation step of buckle or frequency analysis is applied, and eigenvalue extraction procedure is carried out using the Lanczos solver. For the case of vibration analysis for beams under no axial loading (i.e., neither mechanical nor thermal loading), or the case of thermal stability for beams subject to uniform temperature variation, only a buckle analysis is needed to obtain the natural frequency or the critical temperature variation.

**Table 5**
Comparison of non-dimensional natural frequencies $\bar{\omega} = (\omega_m L^2/h)\sqrt{\rho/E_2}$ of a four-layer SS symmetric cross-ply laminated beam ([0°/90°/90°/0°], $E_1/E_2 = 40$, Material 2).*

| L/h | m | Theory | | |
|---|---|---|---|---|
| | | A | $HSPSDT_{ds}$ | $HSPSDT_{cs}$ |
| 5 | 1 | 6.806 | 6.987 (2.659) | 6.845 (0.573) |
| | 2 | 16.515 | 16.892 (2.283) | 16.659 (0.872) |
| | 3 | 26.688 | 27.164 (1.784) | 26.932 (0.914) |
| 10 | 1 | 9.343 | 9.486 (1.531) | 9.370 (0.289) |
| | 2 | 27.224 | 27.947 (2.656) | 27.379 (0.569) |
| | 3 | 46.419 | 47.665 (2.652) | 46.947 (1.137) |
| 20 | 1 | 10.640 | 10.707 (0.630) | 10.662 (0.207) |
| | 2 | 37.374 | 37.944 (1.525) | 37.480 (0.284) |
| | 3 | 71.744 | 73.366 (2.261) | 72.032 (0.401) |
| 100 | 1 | 11.193 | 11.215 (0.197) | 11.213 (0.179) |
| | 2 | 44.477 | 44.589 (0.252) | 44.556 (0.178) |
| | 3 | 98.988 | 99.336 (0.352) | 99.174 (0.188) |

* A: Exact solutions from [51].

As illustrated in Tables 7 and 9, compared with FE simulations, the zigzag HSPSDT theory ($HSPSDT_{cs}$) gives better predictions than the quasi-3D theory of Canales and Mantari [40], for all the boundary conditions considered. Additional FE simulations are also carried out to validate the proposed theory, as shown in Figs. 5–8. Unless otherwise stated, $HSPSDT_{cs}$ is employed in all subsequent discussions.

## 4. Results and discussions

In this section, the quasi-3D zigzag shear deformation beam theory $HSPSDT_{cs}$ is applied to selected free vibration and stability examples. A variety of boundary conditions, geometric parameters and material

**Table 6**
Comparison of non-dimensional natural frequencies $\bar{\omega} = (\omega_m L^2/h)\sqrt{\rho_f/E_{2f}}$ of a thick sandwich beam ([*face*/*core*/*face*], $L/h = 5$, $h_c/h_f = 8$, Material 3).*

| Boundary condition | Theory | m | | |
|---|---|---|---|---|
| | | 1 | 2 | 3 |
| FF | A | 16.072 | 23.631 | 34.324 |
| | $HSPSDT_{ds}$ | 16.679 (3.777) | 24.580 (4.016) | 35.696 (3.997) |
| | $HSPSDT_{cs}$ | 16.091 (0.118) | 23.591 (−0.169) | 34.171 (−0.446) |
| SF | A | 11.307 | 20.961 | 29.974 |
| | $HSPSDT_{ds}$ | 11.722 (3.670) | 21.780 (3.907) | 31.132 (3.863) |
| | $HSPSDT_{cs}$ | 11.305 (−0.018) | 20.919 (−0.200) | 29.878 (−0.320) |
| CF | A | 3.636 | 11.638 | 21.837 |
| | $HSPSDT_{ds}$ | 3.759 (3.383) | 12.137 (4.288) | 22.879 (4.772) |
| | $HSPSDT_{cs}$ | 3.655 (0.523) | 11.739 (0.868) | 22.014 (0.811) |
| SS | A | 7.815 | 17.243 | 26.820 |
| | $HSPSDT_{ds}$ | 8.096 (3.596) | 17.915 (3.897) | 27.830 (3.766) |
| | $HSPSDT_{cs}$ | 7.815 (0.000) | 17.194 (−0.284) | 26.722 (−0.365) |
| CS | A | 8.252 | 17.669 | 27.352 |
| | $HSPSDT_{ds}$ | 8.924 (8.143) | 18.552 (4.997) | 28.682 (4.863) |
| | $HSPSDT_{cs}$ | 8.326 (0.897) | 17.829 (0.906) | 27.587 (0.859) |
| CC | A | 8.965 | 18.084 | 27.917 |
| | $HSPSDT_{ds}$ | 9.442 (5.321) | 19.341 (6.951) | 29.577 (5.946) |
| | $HSPSDT_{cs}$ | 9.070 (1.171) | 18.376 (1.614) | 28.468 (1.974) |

* A: Elasticity solutions from [52].

**Table 7**
Comparison of non-dimensional fundamental frequencies $\bar{\omega} = (\omega L^2/h)\sqrt{\rho/E_2}$ of an angle-ply laminated beam ([0°/θ/0°], $L/h = 10$, $E_1/E_2 = 40$, Material 1)*

| Lamination | Theory | SS | CC | CF | CS | FF | SF |
|---|---|---|---|---|---|---|---|
| 0°/30°/0° | A | 13.882 | 20.242 | 5.580 | 17.005 | 29.916 | 29.934 |
| | HSPSDT$_{cs}$ | 13.792 | 20.033 | 5.562 | 16.496 | 29.703 | 20.785 |
| | FEM | 13.750 | 19.891 | 5.544 | 16.599 | 29.744 | 20.857 |
| 0°/45°/0° | A | 13.780 | 20.050 | 5.542 | 16.858 | 29.687 | 29.704 |
| | HSPSDT$_{cs}$ | 13.586 | 19.580 | 5.500 | 16.401 | 29.230 | 20.458 |
| | FEM | 13.448 | 19.201 | 5.508 | 16.450 | 29.114 | 20.698 |
| 0°/60°/0° | A | 13.689 | 19.860 | 5.512 | 16.716 | 29.408 | 29.497 |
| | HSPSDT$_{cs}$ | 13.385 | 19.121 | 5.443 | 16.331 | 28.764 | 20.135 |
| | FEM | 13.301 | 19.010 | 5.479 | 16.249 | 28.514 | 20.260 |
| 0°/90°/0° | A | 13.610 | 19.672 | 5.491 | 16.580 | 29.295 | 29.313 |
| | HSPSDT$_{cs}$ | 13.283 | 18.767 | 5.389 | 16.279 | 28.310 | 19.825 |
| | FEM | 13.147 | 18.510 | 5.329 | 16.119 | 28.379 | 20.242 |

* A: Results from [40].

properties are considered.

### 4.1. Sandwich and laminated composite beams with different boundary conditions

Consider first the vibration and stability of sandwich and laminated composite beams. For convenience, dimensionless natural frequency $\bar{\omega}$, temperature variation $\overline{\Delta T}$, distributed load $\bar{q}$ and terminal force $\bar{P}$ are introduced, as:

$$\bar{\omega} = \omega \frac{L^2}{h}\sqrt{\frac{\rho}{E_2}},\quad \overline{\Delta T} = \Delta T \alpha_1 \times 10^3,\quad \bar{q} = \frac{qL^3}{10bh^3E_2},\quad \bar{P} = \frac{PL^2}{bh^3E_2} \tag{32}$$

For sandwich beams, $\rho$ and $E_2$ refer to the density and elastic modulus of the face sheets, respectively.

Fig. 3 presents the influence of face-to-beam thickness ratio $h_f/h$ on the fundamental frequencies and critical temperature variations of thick sandwich beams with various boundary conditions. The natural frequencies initially increase rapidly and then gradually decrease as $h_f/h$ is increased; while critical temperature variations decrease monotonously with increasing $h_f/h$.

As for three-layered cross-ply laminated beams with varying boundary conditions, the effect of length-to-thickness ratio $L/h$ on the fundamental frequencies and critical temperature variations are presented in Fig. 4. As $L/h$ is increased to 40, the fundamental frequencies and critical temperature variations rapidly increase and decrease, respectively, both exhibiting an asymptotic behavior when $L/h$ exceeds 40.

The effects of axially distributed load and temperature variation on the fundamental and higher-order frequencies of laminated beams are shown in Figs. 5 and 6. The fundamental frequencies associated with different boundary conditions decrease monotonically to zero when the axially distributed load or temperature variation is increased to the critical buckling one, because the geometric stiffness matrix $[\mathbf{K_G}]$ of Eq. (30) induced by external axial load (i.e., axially distributed load, or thermal stress) increases rapidly as soon as the axially distributed load or the temperature variation reaches to the critical one. In contrast, the higher-order frequencies are not sensitive to the axially distributed load or temperature variation, as shown in Fig. 7.

In Fig. 7a, the buckling capacity of laminated beams under combined axially distributed load and terminal force is depicted. The case of CS shares the same critical terminal load $\overline{P_{cr}}$ with that of SC when the distributed force $\overline{q_{cr}} = 0$, but diverges when $\overline{q_{cr}}$ is increased. The relationship between the distributed load $\overline{q_{cr}}$ and the terminal force $\overline{P_{cr}}$ is nearly linear for the types of boundary conditions considered. It is also noticed that the critical buckling load is higher for stronger end constraints, with the greatest one gained by the beams with CC boundary conditions. As a specific case, Fig. 7b plots further a comprehensive 3D interaction diagram of the fundamental frequency, terminal force and distributed load of a CC laminated beam. Concurrent terminal force and distributed load are seen to cause rapid decrease of the fundamental frequency.

**Table 8**
Comparison of non-dimensional critical temperature variations $\overline{\Delta T_{cr}} = \Delta T_{cr} L^2 \alpha_1/h^2$ of a three-layer cross-ply laminated beam ([0°/90°/0°], $E_1/E_2 = 20$, Material 1).*

| $L/h$ | Theory | Boundary condition | | |
|---|---|---|---|---|
| | | HH | HC | CC |
| 10 | A$_{ds}$ | 0.791 | 1.230 | 1.797 |
| | HSPSDT$_{ds}$ | 0.783 (−1.011) | 1.248 (1.135) | 1.759 (−2.114) |
| | A$_{cs}$ | 0.775 | 1.193 | 1.511 |
| | HSPSDT$_{cs}$ | 0.766 (−1.161) | 1.181 (−1.006) | 1.497 (−0.927) |
| 50 | A$_{ds}$ | 1.049 | 2.110 | 4.030 |
| | HSPSDT$_{ds}$ | 1.036 (−1.240) | 2.049 (−2.891) | 3.906 (−3.077) |
| | A$_{cs}$ | 1.048 | 2.105 | 3.842 |
| | HSPSDT$_{cs}$ | 1.024 (−2.290) | 2.081 (−1.140) | 3.796 (−1.197) |

* A: Results from [18].

### 4.2. Micromechanics-based thermo-mechanical model with hinged-hinged boundary condition

Different from the previous case of laminated beams with specified material properties, a micromechanics-based thermo-mechanical model is employed in this subsection. The material parameters can be systematically varied by varying the fiber volume fraction $V_f$ (or the matrix volume fraction $V_m = 1 - V_f$). In the micromechanical model, the fibers are assumed transversely isotropic while the matrix is assumed isotropic. The effective material properties of a fiber-reinforced composite (FRC) can be written as [54]:

$$\begin{aligned}
&E_1 = E_{f1}V_f + E_mV_m,\quad E_2 = \frac{E_{f2}E_m}{E_mV_f + E_{f2}V_m},\quad E_3 = E_2,\\
&G_{12} = \frac{G_{f12}G_m}{G_mV_f + G_{f12}V_m},\quad G_{13} = G_{12},\quad G_{23} = \frac{E_3}{2(1+\upsilon_{23})},\\
&\upsilon_{12} = \upsilon_{f12}V_f + \upsilon_mV_m,\quad \upsilon_{13} = \upsilon_{12},\quad \upsilon_{23} = \frac{E_{f2}V_m\upsilon_m + E_mV_f\upsilon_{f23}}{E_mV_f + E_{f2}V_m},\\
&\alpha_1 = \frac{\alpha_{f1}E_{f1}V_f + \alpha_mE_mV_m}{E_{f1}V_f + E_mV_m},\quad \alpha_2 = (\alpha_{f2} + \upsilon_{f12}\alpha_{f1})V_f + (1+\upsilon_m)\alpha_mV_m\\
&\qquad -(\upsilon_{f12}V_f + \upsilon_mV_m)\alpha_1,\\
&\alpha_3 = \alpha_2,\quad \rho = \rho_fV_f + \rho_mV_m
\end{aligned} \tag{33}$$

Based upon the micromechanical model, a three-layered cross-ply

**Table 9**
Comparison of non-dimensional critical buckling load $P_{cr}L^2/(bh^3E_2)$ of an angle-ply laminated beam ([0°/θ/0°], $L/h = 10$, $E_1/E_2 = 40$, Material 1).*

| Lamination | Theory | Boundary condition | | | |
|---|---|---|---|---|---|
| | | SS | CC | CF | CS |
| 0°/30°/0° | A | 19.614 | 36.260 | 6.882 | 27.165 |
| | HSPSDT$_{cs}$ | 19.574 | 36.308 | 6.836 | 27.429 |
| | FEM | 19.514 | 36.051 | 6.814 | 27.600 |
| 0°/45°/0° | A | 19.319 | 35.598 | 6.796 | 26.707 |
| | HSPSDT$_{cs}$ | 19.285 | 35.557 | 6.725 | 26.464 |
| | FEM | 19.089 | 35.368 | 6.703 | 26.543 |
| 0°/60°/0° | A | 19.060 | 34.933 | 6.732 | 26.265 |
| | HSPSDT$_{cs}$ | 19.032 | 34.769 | 6.625 | 25.806 |
| | FEM | 18.877 | 34.593 | 6.669 | 25.617 |
| 0°/90°/0° | A | 18.829 | 34.263 | 6.692 | 25.835 |
| | HSPSDT$_{cs}$ | 18.761 | 34.009 | 6.604 | 25.231 |
| | FEM | 18.569 | 33.843 | 6.576 | 25.461 |

* A: Results from [40].

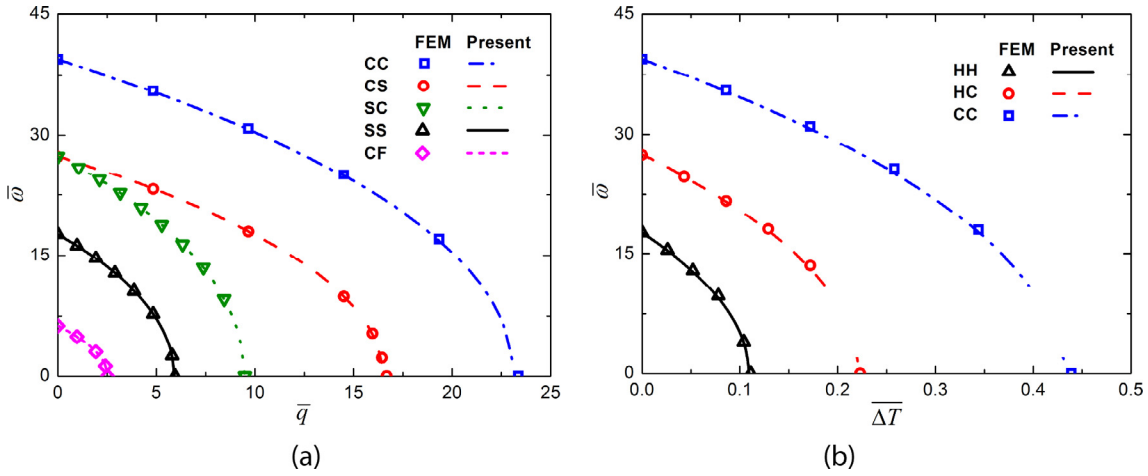


**Fig. 5.** Effects of (a) axially distributed load and (b) temperature variation on fundamental frequency of a laminated beam ([0°/90°/0°], $L/h = 100$, Material 1).

FRC laminated beam with hinged-hinged boundary conditions is considered, for which the fiber volume fraction of each ply is identical. As listed in Table 3 (see Material 3), the materials properties are temperature-dependent for the matrix, but temperature-independent for the fiber with a negative coefficient of thermal expansion along the fiber direction. Both the cases considering temperature-independent and temperature-dependent material properties are discussed, which are referred to below as TI and TD cases, respectively. For the latter case (TD), an iterative procedure is utilized to obtain convergent critical temperature variations.

Fig. 8 shows the influence of fiber volume fraction on fundamental frequency $\bar{\omega}$ and critical temperature variation $\Delta T_{cr}$ of the HH laminated beam as predicted by the micromechanical model. As shown in Fig. 8a, the fundamental frequency $\bar{\omega}$ under selected temperature variations $\Delta T$ increases with increasing $V_f$. The TI case gives higher predictions of $\bar{\omega}$ and $\Delta T_{cr}$ than the TD case. As $V_f$ is increased, the difference in the two cases tends to vanish, attributed to the decreased volume fraction of the TD matrix. It is interesting to notice that, as $\Delta T$ is increased, $\bar{\omega}$ decreases when $V_f < 0.37$, but increases when $V_f > 0.37$. With $V_f = 0.37$, $\bar{\omega}$ seems insensitive to $\Delta T$. Correspondingly, as shown in Fig. 8b, the relationship between $\Delta T_{cr}$ and $V_f$ is approximately hyperbolic, with $\Delta T_{cr}$ converging towards positive or negative infinity when $V_f$ approaches 0.37. The laminated beam buckles upon heating when $V_f < 0.37$, but buckles upon cooling when $V_f > 0.37$, which is attributed to the appearance of negative $\alpha_2/\alpha_1$ at large $V_f$. As $V_f$ reaches 0.37, the laminated beam may not buckle whether they are heated or cooled, *i.e.*, the so-called *non-thermal buckling* occurs. For specific material properties, the axial thermal loading $N_x^T$ as shown in Eq. (21) may vanish, thus causing the *non-thermal buckling*. Similar behaviors were observed for composite plates and beams [18,55].

### 4.3. Fiber metal laminated (FML) beams with hinged-hinged boundary condition

The FML beams studied here are hinged-hinged symmetric GLARE beams, which are consisted of cross-ply glass fiber-reinforced plastic (polyster) composite (GFRP) and aluminum (Al) layers, with material properties listed in Table 3. The GFRP has a lay-up of $[0°/90°/0°/90°/0°]_s$. Each FML beam has 10 layers that are numbered from top to bottom, of which only 2 are Al layers. The 2 Al layers are placed symmetrically in the FML, with their positions systematically varied as (1, 10), (2, 9), (3, 8), (4, 7), and (5, 6) to evaulate their position effect on free vibration and stability of the FML structure.

Fig. 9a and b present separately the effects of Al layer stacking sequence and length-to-thickness ratio of the structure on the fundamental frequency (under thermal loading) and critical temperature

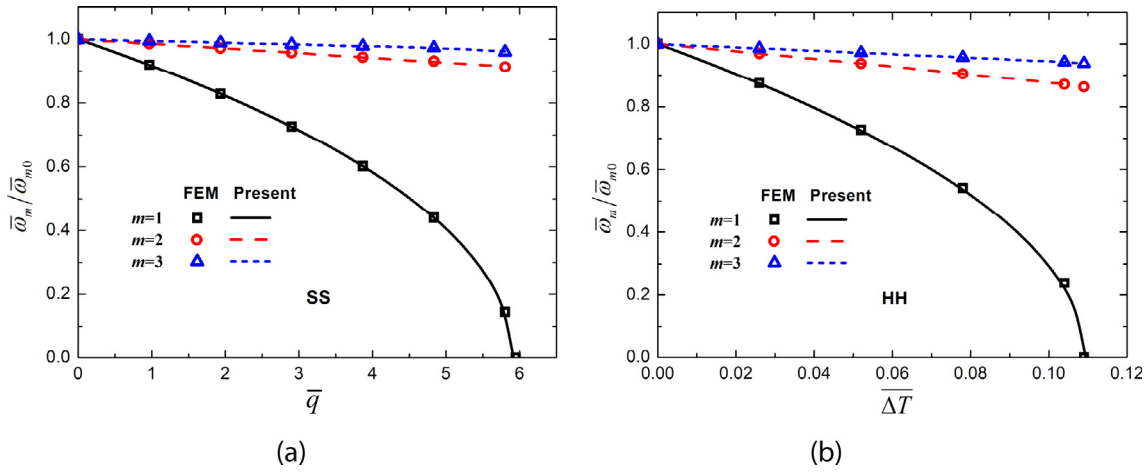


**Fig. 6.** Effects of (a) axially distributed load and (b) temperature variation on the first three natural frequencies (normalized by the corresponding frequency $\bar{\omega}_{m0}$ without mechanical or thermal loading) of a SS/HH laminated beam ([0°/90°/0°], $L/h = 100$, Material 1). The parameter $m$ refers to the number of vibration modal.

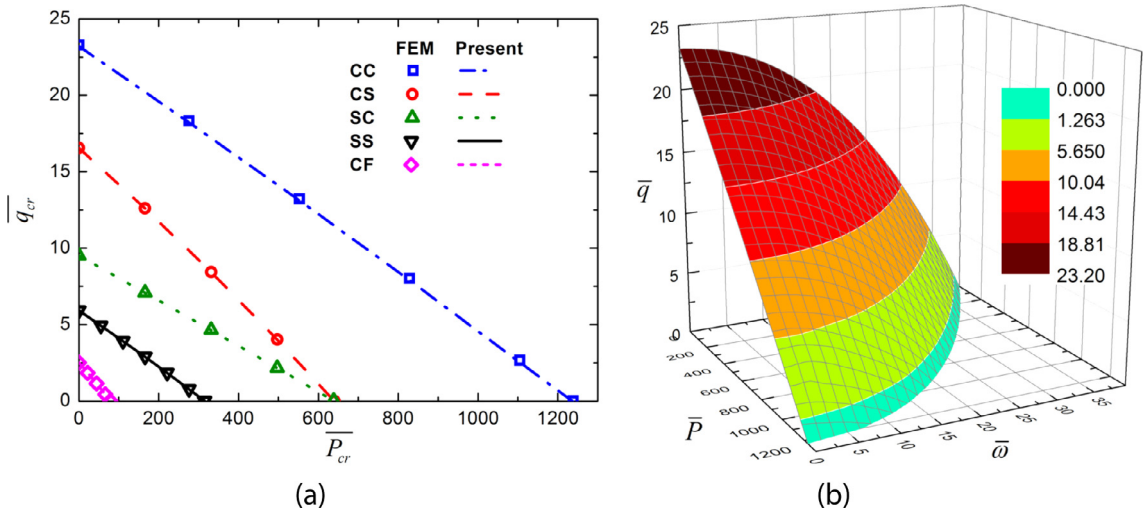


**Fig. 7.** (a) Buckling capacity of laminated beams under combined axially distributed load and terminal force; (b) fundamental frequency - terminal force – distributed load interaction curves of a CC laminated beam ([0°/90°/0°], $L/h = 100$, Material 1).

variation of FML beams. For reference, the case that no Al layers are inserted is also included. The results of Fig. 9 demonstrate that, replacing only the outer layers (i.e., layers (1, 10)) of a 10-layer GFRP laminated beam with the Al layers leads to the highest fundamental frequency and critical temperature variation, since this arrangement of the Al layers with the highest elastic modulus (see Material 5 of Table 3) can always result in the maximum flexural rigidity, which maximizes the structural stiffness matrix [**K**]. Interestingly, this conclusion coincides with the previous finding that placing Al sheets in the outer layers always results in the best impact resistance of the FML [56,57]. In other words, these results imply that placing Al sheets in the outer layers of a FML structure enables it to exhibit the highest fundamental frequency, best thermal buckling and impact resistance.

## 5. Conclusions

A generalized refined quasi-3D zigzag beam theory, with consideration of thickness stretching and interlaminar continuity of both transverse shear stress and displacements, has been developed to study the free vibration and buckling behaviors of multilayered composite beams subjected to axially distributed load, terminal force and/or uniform thermal loading. A combined hyperbolic sinusoidal and polynomial shear shape function was employed to construct the theory. The types of composite beam considered included laminated composite beams, sandwich beams with composite face sheets, and fiber metal laminates (FML). Solutions were obtained for different boundary conditions by using the Ritz method in terms of boundary characteristic orthogonal polynomial functions. For validation, the theoretical predictions were compared with exiting results and the present FE simulations, and good agreements were achieved. The effects of axially distributed force and terminal load, together with temperature variation on free vibration and buckling of the composite beam were quantified for various boundary conditions, geometric parameters and material properties. It has been demonstrated that the proposed theory can be considered as an appropriate and highly efficient method for analyzing the vibration and stability behaviors of various multilayered beams under mechanical/thermal loadings.

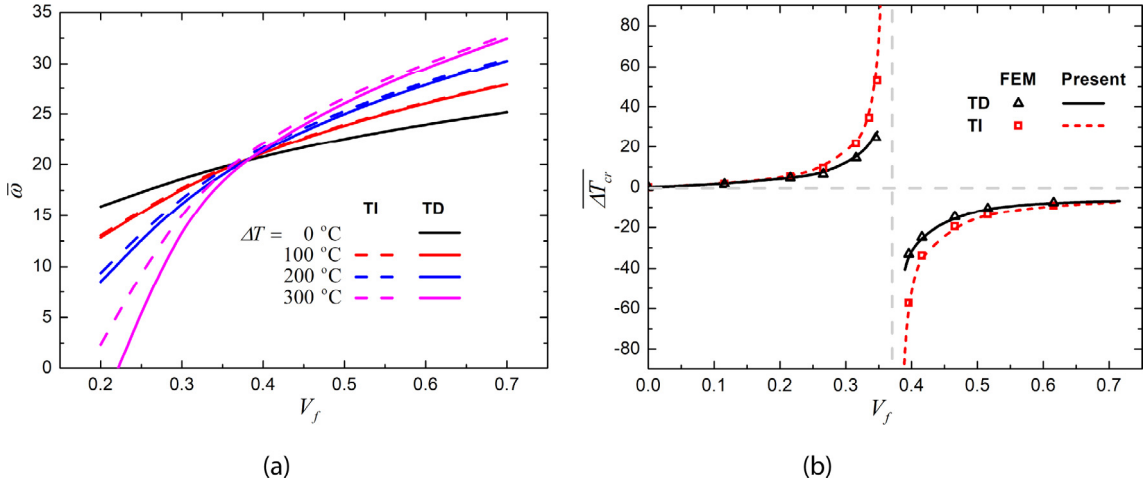


**Fig. 8.** Effect of fiber volume fraction on (a) fundamental frequency $\bar{\omega} = \omega L^2/h(\rho_m/E_m)^{1/2}$ and (b) critical temperature variation $\overline{\Delta T_{cr}} = \Delta T_{cr} L^2 \alpha_{f2}/h^2$ of a HH laminated beam based upon the micromechanical model ([0°/90°/0°], $L/h = 50$, Material 4; TI and TD refer to the cases of temperature-independent and temperature-dependent material properties, respectively).

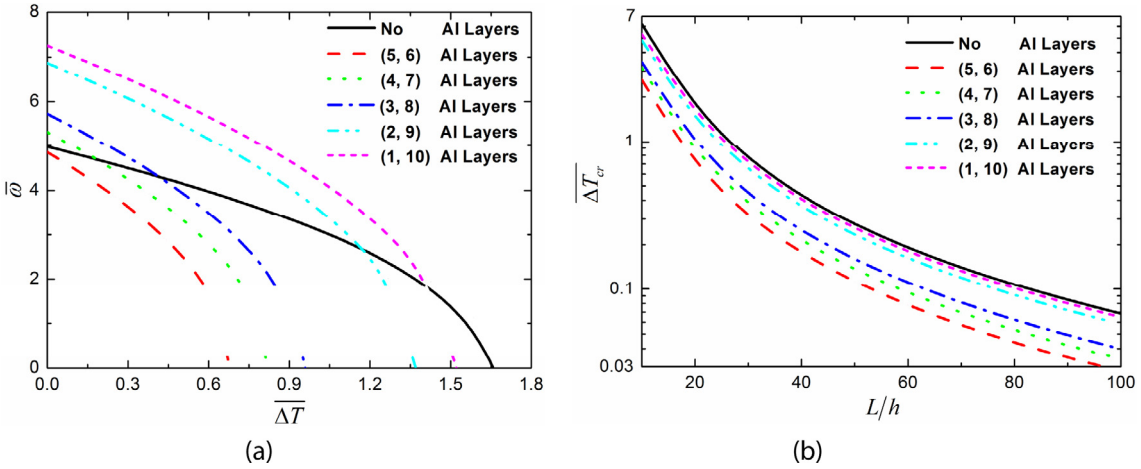


**Fig. 9.** (a) Effect of temperature variation $\overline{\Delta T} = 1000\alpha_{1f}\Delta T$ on fundamental frequency $\bar{\omega} = (\omega L^2/h)\sqrt{\rho_f/E_{2f}}$ $(L/h = 20)$, and (b) effect of length-to-thickness ratio $L/h$ on critical temperature variation $\overline{\Delta T_{cr}}$ of HH FML beams with different Al layer sequences (Material 5). The subscript $f$ refers to the corresponding material properties of GFRP.


## Acknowledgments

This work was supported by the National Natural Science Foundation of China (51375369, 11472209, 11702326 and 11472208), China Postdoctoral Science Foundation (2016M600782), Postdoctoral Scientific Research Project of Shaanxi Province (2016BSHYDZZ18), Zhejiang Provincial Natural Science Foundation of China (LGG18A020001), Natural Science Basic Research Plan in Shaanxi Province of China (2018JQ1078), and the Fundamental Research Funds for Xi'an Jiaotong University (xjj2015102).


## Appendix A. Elements of [K], [M], and [$K_G$] matrices

The structural stiffness matrix is

$$[K] = \begin{bmatrix} K^{cc} & K^{cd} & K^{ce} & K^{cf} \\ K^{cd} & K^{dd} & K^{de} & K^{df} \\ K^{ce} & K^{de} & K^{ee} & K^{ef} \\ K^{cf} & K^{df} & K^{ef} & K^{ff} \end{bmatrix} \tag{A.1}$$

where

$$\begin{aligned} K_{ij}^{cc} &= \int_0^L A_{11}\phi_{i,x}^c\phi_{j,x}^c dx \\ K_{ij}^{cd} &= -\int_0^L A_{11}^b\phi_{i,x}^c\phi_{j,x}^d dx \\ K_{ij}^{ce} &= -\int_0^L A_{11}^s\phi_{i,x}^c\phi_{j,x}^e dx \\ K_{ij}^{cf} &= \int_0^L (L_1\phi_{i,x}^c\phi_j^f - A_{11}^{st}\phi_{i,x}^c\phi_{j,x}^f) dx \\ K_{ij}^{dd} &= \int_0^L B_{11}^b\phi_{i,xx}^d\phi_{j,xx}^d dx \\ K_{ij}^{de} &= \int_0^L B_{11}^s\phi_{i,xx}^d\phi_{j,xx}^e dx \\ K_{ij}^{df} &= \int_0^L (B_{11}^{st}\phi_{i,xx}^d\phi_{j,xx}^f - L_1^b\phi_{i,xx}^d\phi_j^f) dx \\ K_{ij}^{ee} &= \int_0^L (C_{11}^s\phi_{i,xx}^e\phi_{j,xx}^e + A_{55}^s\phi_{i,x}^e\phi_{j,x}^e) dx \\ K_{ij}^{ef} &= \int_0^L (C_{11}^{st}\phi_{i,xx}^e\phi_{j,xx}^f - L_1^s\phi_{i,xx}^e\phi_j^f + A_{55}^s\phi_{i,x}^e\phi_{j,x}^f) dx \\ K_{ij}^{ff} &= \int_0^L (D_{11}^{st}\phi_{i,xx}^f\phi_{j,xx}^f - L_1^{st}\phi_{i,xx}^f\phi_j^f + R^s\phi_i^f\phi_j^f + A_{55}^s\phi_{i,x}^f\phi_{j,x}^f) dx \end{aligned} \tag{A.2}$$

The geometric stiffness matrix induced by external axial load is

$$[K_G] = \begin{bmatrix} 0 & 0 & 0 & 0 \\ 0 & K^{ddg} & K^{deg} & K^{dfg} \\ 0 & K^{deg} & K^{eeg} & K^{efg} \\ 0 & K^{dfg} & K^{efg} & K^{ffg} \end{bmatrix} \tag{A.3}$$

where

$$
\begin{aligned}
K_{ij}^{ddg} &= \int_0^L \hat{N}_x \phi_{i,x}^d \phi_{j,x}^d \mathrm{d}x \\
K_{ij}^{deg} &= \int_0^L \hat{N}_x \phi_{i,x}^d \phi_{j,x}^e \mathrm{d}x \\
K_{ij}^{dfg} &= \int_0^L \hat{N}_x g(0) \phi_{i,x}^d \phi_{j,x}^f \mathrm{d}x \\
K_{ij}^{eeg} &= \int_0^L \hat{N}_x \phi_{i,x}^e \phi_{j,x}^e \mathrm{d}x \\
K_{ij}^{efg} &= \int_0^L \hat{N}_x g(0) \phi_{i,x}^e \phi_{j,x}^f \mathrm{d}x \\
K_{ij}^{ffg} &= \int_0^L \hat{N}_x g^2(0) \phi_{i,x}^f \phi_{j,x}^f \mathrm{d}x
\end{aligned} \tag{A.4}
$$

The mass matrix is

$$
[\mathrm{M}] = \begin{bmatrix} \mathrm{M}^{cc} & \mathrm{M}^{cd} & \mathrm{M}^{ce} & \mathrm{M}^{cf} \\ \mathrm{M}^{cd} & \mathrm{M}^{dd} & \mathrm{M}^{de} & \mathrm{M}^{df} \\ \mathrm{M}^{ce} & \mathrm{M}^{de} & \mathrm{M}^{ee} & \mathrm{M}^{ef} \\ \mathrm{M}^{cf} & \mathrm{M}^{df} & \mathrm{M}^{ef} & \mathrm{M}^{ff} \end{bmatrix} \tag{A.5}
$$

where

$$
\begin{aligned}
M_{ij}^{cc} &= \int_0^L I_{11} \phi_i^c \phi_j^c \mathrm{d}x \\
M_{ij}^{cd} &= \int_0^L I_{12} \phi_i^c \phi_{j,x}^d \mathrm{d}x \\
M_{ij}^{ce} &= \int_0^L I_{13} \phi_i^c \phi_{j,x}^e \mathrm{d}x \\
M_{ij}^{cf} &= \int_0^L I_{14} \phi_i^c \phi_{j,x}^f \mathrm{d}x \\
M_{ij}^{dd} &= \int_0^L (I_{22} \phi_{i,x}^d \phi_{j,x}^d + I_{55} \phi_i^d \phi_j^d) \mathrm{d}x \\
M_{ij}^{de} &= \int_0^L (I_{33} \phi_{i,x}^d \phi_{j,x}^e + I_{55} \phi_i^d \phi_j^e) \mathrm{d}x \\
M_{ij}^{df} &= \int_0^L (I_{24} \phi_{i,x}^d \phi_{j,x}^f + I_{56} \phi_i^d \phi_j^f) \mathrm{d}x \\
M_{ij}^{ee} &= \int_0^L (I_{33} \phi_{i,x}^e \phi_{j,x}^e + I_{55} \phi_i^e \phi_j^e) \mathrm{d}x \\
M_{ij}^{ef} &= \int_0^L (I_{34} \phi_{i,x}^e \phi_{j,x}^f + I_{56} \phi_{i,}^e \phi_j^f) \mathrm{d}x \\
M_{ij}^{ff} &= \int_0^L (I_{44} \phi_{i,x}^f \phi_{j,x}^f + I_{66} \phi_i^f \phi_j^f) \mathrm{d}x
\end{aligned} \tag{A.6}
$$

## Appendix B. Supplementary data

Supplementary data associated with this article can be found, in the online version, at https://doi.org/10.1016/j.compstruct.2018.08.005.

## References


[1] Botelho EC, Silva RA, Pardini LC, Rezende MC. A review on the development and properties of continuous fiber/epoxy/aluminum hybrid composites for aircraft structures. Mater Res 2006;9(3):247–56.
[2] Vermeeren C. Around GLARE, A New Aircraft Material in Context. Kluwer Academic Publishers; 2004.
[3] Shooshtari A, Razavi S. A closed form solution for linear and nonlinear free vibrations of composite and fiber metal laminated rectangular plates. Compos Struct 2010;92(11):2663–75.
[4] Payeganeh GH, Ghasemi FA, Malekzadeh K. Dynamic response of fiber-metal laminates (FMLs) subjected to low-velocity impact. Thin-Walled Struct 2010;48(1):62–70.
[5] Fu YM, Chen Y, Zhong J. Analysis of nonlinear dynamic response for delaminated fiber-metal laminated beam under unsteady temperature field. J Sound Vib 2014;333(22):5803–16.
[6] Fu YM, Tao C. Nonlinear dynamic responses of viscoelastic fiber-metal-laminated beams under the thermal shock. J Eng Math 2016;98(1):113–28.
[7] Tao C, Fu YM, Dai HL. Nonlinear dynamic analysis of fiber metal laminated beams subjected to moving loads in thermal environment. Compos Struct 2016;140:410–6.
[8] Han B, Li FH, Ni CY, Zhang QC, Chen CQ, Lu TJ. Stability and initial post-buckling analysis of a standing sandwich beam under terminal force and self-weight. Arch Appl Mech 2016;86(6):1063–82.
[9] Virgin LN. Vibration of Axially Loaded Structures. New York: Cambridge University Press; 2007.
[10] Naguleswaran S. Vibration of a vertical cantilever with and without axial freedom at clamped end. J Sound Vib 1991;146:191–8.
[11] Virgin LN, Santillan ST, Holland DB. Effect of gravity on the vibration of vertical cantilevers. Mech Res Commun 2007;34:312–7.
[12] Hijmissen JW, van Horssen WT. On aspect of damping for a vertical beam with a tuned mass damper at the top. Nonlinear Dynam 2007;50(1):169–90.
[13] Hijmissen JW, van Horssen WT. On transverse vibrations of a vertical Timoshenko beam. J Sound Vib 2008;314:161–79.
[14] Abramovich H. Free vibrations of gravity loaded composite beams. Compos Struct 1993;23(1):17–26.
[15] Xi LY, Li XF, Tang GJ. Free vibration of standing and hanging gravity-loaded Rayleigh cantilevers. Int J Mech Sci 2013;66:233–8.
[16] Pai PF. A new look at shear correction factors and warping functions of anisotropic laminates. Int J Solids Struct 1995;32(16):2295–313.
[17] Nallim LG, Oller S, Onate E, Flores FG. A hierarchical finite element for composite laminated beams using a refined zigzag theory. Compos Struct 2017;163:168–84.
[18] Aydogdu M. Thermal buckling analysis of cross-ply laminated composite beams with general boundary conditions. Compos Sci Technol 2007;67(6):1096–104.
[19] Aydogdu M. Vibration analysis of cross-ply laminated beams with general boundary conditions by Ritz method. Int J Mech Sci 2005;47(11):1740–55.
[20] Vidal P, Polit O. Vibration of multilayered beams using sinus finite elements with transverse normal stress. Compos Struct 2010;92(6):1524–34.
[21] Sayyad AS, Ghugal YM. Bending, buckling and free vibration of laminated composite and sandwich beams: a critical review of literature. Compos Struct 2017;171:486–504.
[22] Shao D, Hu SH, Wang QS, Pang FZ. Free vibration of refined higher-order shear deformation composite laminated beams with general boundary conditions. Compos Part B-Eng 2017;108:75–90.
[23] Aydogdu M, Taskin V. Free vibration analysis of functionally graded beams with simply supported edges. Mater Des 2007;28(5):1651–6.
[24] Vo TP, Thai HT, Nguyen TK, Inam F, Lee J. A quasi-3D theory for vibration and buckling of functionally graded sandwich beams. Compos Struct 2015;119:1–12.
[25] Wattanasakulpong N, Prusty BG, Kelly DW, Hoffman M. Free vibration analysis of layered functionally graded beams with experimental validation. Mater Des 2012;36:182–90.
[26] Léotoing L, Drapier S, Vautrin A. Nonlinear interaction of geometrical and material properties in sandwich beam instabilities. Int J Solids Struct 2002;39:3717–39.
[27] Yu K, Hu H, Chen SY, Belouettar S, Potier-Ferry M. Multi-scale techniques to analyze instabilities in sandwich structures. Compos Struct 2013;96:751–62.
[28] Sad Saoud K, Le Grognec PL. Post-buckling analysis of elastoplastic sandwich columns by means of an enriched 1D finite element model. Int J Solids Struct 2017;129:90–102.

[29] Carrera E. Historical review of zig-zag theories for multilayered plates and shells. Appl Mech Rev 2003;56(3):287–308.
[30] Kapuria S, Dumir PC, Jain NK. Assessment of zigzag theory for static loading, buckling, free and forced response of composite and sandwich beams. Compos Struct 2004;64(3–4):317–27.
[31] Hu H, Belouettar S, Potier-Ferry M. Review and assessment of various theories for modeling sandwich composites. Compos Struct 2008;84(3):282–92.
[32] Carrera E, Filippi M, Zappino E. Free vibration analysis of laminated beam by polynomial, trigonometric, exponential and zig-zag theories. J Compos Mater 2014;48(19):2299–316.
[33] Carrera E, Filippi M, Zappino E. Laminated beam analysis by polynomial, trigonometric, exponential and zig-zag theories. Eur J Mech A-Solid 2013;41:58–69.
[34] Tessler A, Di Sciuva M, Gherlone M. A refined zigzag beam theory for composite and sandwich beams. J Compos Mater 2009;43(9):1051–81.
[35] Di Sciuva M, Gherlone M, Iurlaro L, Tessler A. A class of higher-order $C^0$ composite and sandwich beam elements based on the Refined Zigzag theory. Compos Struct 2015;132:784–803.
[36] Treviso A, Mundo D, Tournour M. A $C^0$-continuous RZT beam element for the damped response of laminated structures. Compos Struct 2015;131:987–94.
[37] Carrera E, Giunta G, Petrolo M. Beam Structures: Classical and Advanced Theories. John Wiley & Sons; 2011.
[38] Matsunaga H. Vibration and buckling of multilayered composite beams according to higher order deformation theories. J Sound Vib 2001;246:47–62.
[39] Mantari JL, Canales FG. Free vibration and buckling of laminated beams via hybrid Ritz solution for various penalized boundary conditions. Compos Struct 2016;152:306–15.
[40] Canales FG, Mantari JL. Buckling and free vibration of laminated beams with arbitrary boundary conditions using a refined HSDT. Compos Part B-Eng 2016;100:136–45.
[41] Vo TP, Thai HT, Nguyen TK, Inam F, Lee J. Static behaviour of functionally graded sandwich beams using a quasi-3D theory. Compos Part B-Eng 2015;68:59–74.
[42] Vo TP, Thai HT, Aydogdu M. Free vibration of axially loaded composite beams using a four-unknown shear and normal deformation theory. Compos Struct 2017;178:406–14.
[43] Nguyen TK, Vo TP, Nguyen BD, Lee J. An analytical solution for buckling and vibration analysis of functionally graded sandwich beams using a quasi-3D shear deformation theory. Compos Struct 2016;156:238–52.
[44] Osofero AI, Vo TP, Nguyen TK, Lee J. Analytical solution for vibration and buckling of functionally graded sandwich beams using various quasi-3D theories. J Sandw Struct Mater 2016;18(1):3–29.
[45] Zhen W, Wanji C. Free vibration of laminated composite and sandwich plates using global–local higher-order theory. J Sound Vib 2006;298(1):333–49.
[46] Iurlaro L, Gherlone M, Di Sciuva M, Tessler A. Assessment of the refined zigzag theory for bending, vibration, and buckling of sandwich plates: a comparative study of different theories. Compos Struct 2013;106:777–92.
[47] Reddy JN. Mechanics of Laminated Composite Plates and Shells: Theory and Analysis. CRC Press; 2004.
[48] Houari MSA, Tounsi A, Bég OA. Thermoelastic bending analysis of functionally graded sandwich plates using a new higher order shear and normal deformation theory. Int J Mech Sci 2013;76:102–11.
[49] Han B, Qin KK, Zhang QC, Zhang Q, Lu TJ, Lu BH. Free vibration and buckling of foam-filled composite corrugated sandwich plates under thermal loading. Comput Struct 2017;172:173–89.
[50] Narita Y. Combinations for the free-vibration behaviors of anisotropic rectangular plates under general edge conditions. J Appl Mech-T ASME 2000;67(3):568–73.
[51] Pagano N. Exact solutions for composite laminates in cylindrical bending. Mechanics of Composite Materials. Springer; 1994. p. 72–85.
[52] Ye T, Jin G. Elasticity solution for vibration of generally laminated beams by a modified Fourier expansion-based sampling surface method. Comput Struct 2016;167:115–30.
[53] Li FH, Han B, Zhang QC, Jin F, Lu TJ. Buckling of a standing corrugated sandwich plate subjected to body force and terminal load. Thin Wall Struct 2018;127:688–99.
[54] Herakovich C. Mechanics of Fibrous Composites. NewYork: Wiley; 1998.
[55] Jones RM. Thermal buckling of uniformly heated unidirectional and symmetric cross-ply laminated fiber-reinforced composite uniaxial in-plane restrained simply supported rectangular plates. Compos Part A-Appl S 2005;36(10):1355–67.
[56] Abdullah MR, Cantwell WJ. The impact resistance of polypropylene-based fibre-metal laminates. Compos Sci Technol 2006;66(11–12):1682–93.
[57] Sinmazcelik T, Avcu E, Bora MO, Coban O. A review: Fibre metal laminates, background, bonding types and applied test methods. Mater Des 2011;32(7):3671–85.